AM205: Assignment 3 solutions*

Problem 1 – convergence rates of two integrals

Part (a)

As discussed in class, the trapezoidal integration method has the form

$$I_A \approx h\left(\frac{1}{2}f(x_0) + f(x_1) + f(x_2) + ... + f(x_{n-1}) + \frac{1}{2}f(x_n)\right). \tag{1}$$

To compute the error bound, we need to calculate the second derivative of f. We have

$$\frac{d^2f}{dx^2} = \frac{\cos x(\frac{5}{4} - \cos x)^2 - 2\sin^2 x(\frac{5}{4} - \cos x)}{(\frac{5}{4} - \cos x)^4}. \tag{2}$$

The left panel of Fig. 1 shows the error bound and error versus h on a log–log scale. The error bound is always larger than the error. In addition, the slope of error versus h is 2, which verifies that the trapezoidal method is second-order accurate.

Part (b)

This part is analogous to part (a), except that the error decays exponentially with h. In this case, we observe trapezoidal method has exponential convergence (faster than $O(h^m)$ for any m). This is due to a special property of the trapezoidal rule when evaluating periodic integrals. The right panel of Fig. 1 shows the error bound and error versus h on a log–log scale.

Part (c)

Here, we show that

$$I_B = \int_0^{2\pi} f(x)dx = \int_0^{2\pi} \frac{dx}{\frac{5}{4} - \cos x} = \frac{8\pi}{3} \tag{3}$$

using the residue theorem. If $z = e^{i\theta}$ then $\cos\theta = \frac{z+z^{-1}}{2}$. The denominator of the integral in Eq. 3 can be rewritten as

$$\frac{5}{4} - \cos\theta = \frac{5}{4} - \frac{z+z^{-1}}{2} = \frac{5}{4} - \frac{z^2+1}{2z} = \frac{-z^2+2az-1}{2z}. \tag{4}$$

Substituting this expression into the integral transforms it to

$$\oint_C \frac{1}{i}\frac{2dz}{z^2 - \frac{5}{2}z + 1}, \tag{5}$$

*Solutions to problems 1, 2, and 4 were written by Kevin Chen. Solutions to problems 3, 5 and 6 were written by Chris H. Rycroft. Edited by Chris H. Rycroft.

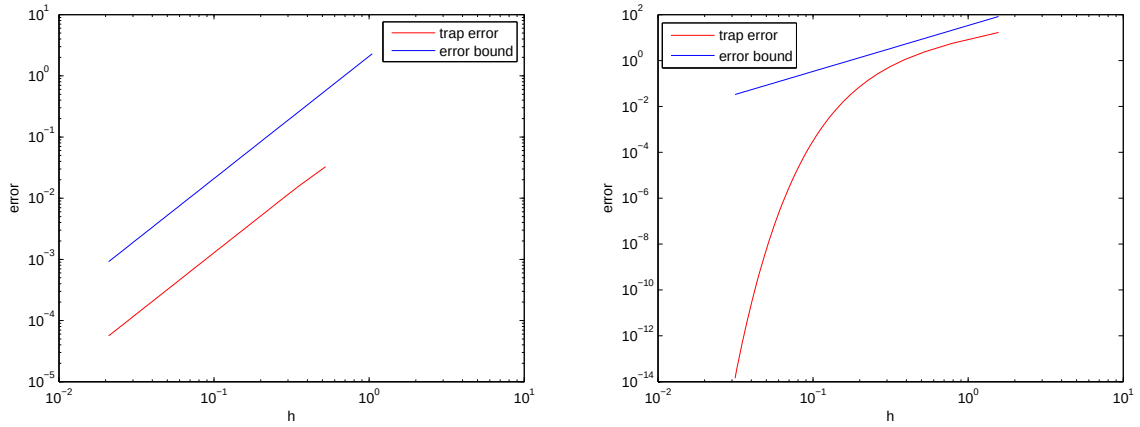

Figure 1: Errors and error bounds as a function of the integration step size h for the two integrals considered in problem 1. The left panel shows results for $\int_0^{\pi/3} f(x)dx$ and the right panel shows results for $\int_0^{2\pi} f(x)dx$.

where the closed contour C represents unit circle in the complex plane. The integrand has two poles at $z = 2$ and $z = \frac{1}{2}$, and only the pole inside the closed contour contributes to the integral. Invoking the residual theorem yields the result

$$I_B = 2\pi i \,\mathrm{Res}\left(\frac{1}{i}\frac{2dz}{z^2 - \frac{5}{2}z + 1}, z = \frac{1}{2}\right) = \frac{8\pi}{3}. \tag{6}$$

Problem 2 – adaptive integration

Part (a) – 3-point Gauss quadrature

The third Legendre polynomial is $P_3(x) = \frac{1}{2}x(5x^2 - 3)$, which has roots at

$$x_1 = -\sqrt{\frac{3}{5}}, \qquad x_2 = 0, \qquad x_3 = \sqrt{\frac{3}{5}}.$$

We now solve for the weights by integrating the Lagrange interpolation polynomials through these three points. We have

$$\begin{aligned} w_0 &= \int_{-1}^{1} L_o(x)dx = \int_{-1}^{1} \frac{x-0}{-\sqrt{3/5}-0} \times \frac{x-\sqrt{3/5}}{-\sqrt{3/5}-\sqrt{3/5}}dx \\ &= \frac{5}{6}\int_{-1}^{1}(x^2 - \sqrt{3/5}x)dx = \frac{5}{6}\int_{-1}^{1}(x^2)dx \\ &= \frac{5}{6}\frac{2}{3} = \frac{5}{9}. \end{aligned} \tag{7}$$

Similarly, we can do the integral for w_1 to obtain

$$\begin{aligned} w_1 &= \int_{-1}^{1} L_1(x)dx = \int_{-1}^{1} \frac{x+\sqrt{3/5}}{+\sqrt{3/5}} \times \frac{x-\sqrt{3/5}}{-\sqrt{3/5}} dx \\ &= -\frac{5}{3}\int_{-1}^{1} \left(x^2 - \frac{3}{5}\right) dx = -\frac{5}{3}\left(\frac{2}{3} - \frac{6}{5}\right) \\ &= -\frac{5}{3}\left(-\frac{8}{15}\right) = \frac{8}{9}. \end{aligned} \tag{8}$$

Finally, w_2 is given by

$$\begin{aligned} w_2 &= \int_{-1}^{1} L_2(x)dx = \int_{-1}^{1} \frac{x-0}{\sqrt{3/5}-0} \times \frac{x+\sqrt{3/5}}{\sqrt{3/5}+\sqrt{3/5}} dx \\ &= \frac{5}{6}\int_{-1}^{1} (x^2 + \sqrt{3/5}x)dx = \frac{5}{6}\int_{-1}^{1} (x^2)dx \\ &= \frac{5}{6}\frac{2}{3} = \frac{5}{9}, \end{aligned} \tag{9}$$

and therefore $[w_0, w_1, w_2] = [\frac{5}{9}, \frac{8}{9}, \frac{5}{9}]$. We now show that this quadrature rule integrates polynomials of up to degree 5 exactly. We show this property on $[-1, 1]$, and if it holds there, it holds on any arbitray interval by performing an affine transformation. An arbitrary fifth-order polynomial can be written as

$$p_5(x) = a + bx + cx^2 + dx^3 + ex^4 + fx^5. \tag{10}$$

We can integrate $p_5(x)$ on $[-1, 1]$ and obtain

$$\begin{aligned} \int_{-1}^{1} p_5(x)dx = a\int_{-1}^{1} dx + b\int_{-1}^{1} xdx + c\int_{-1}^{1} x^2dx \\ + d\int_{-1}^{1} x^3dx + e\int_{-1}^{1} x^4dx + f\int_{-1}^{1} x^5dx. \end{aligned} \tag{11}$$

We can evaluate the simple integrals and arrive at

$$\int_{-1}^{1} p_5(x)dx = 2a + \frac{2c}{3} + \frac{2e}{5}. \tag{12}$$

Evaluating the integral using the weights and quadrature points we obtained gives

$$\begin{aligned} \int_{-1}^{1} p_5(x)dx = \tfrac{5}{9}(a - (\tfrac{3}{5})^{1/2}b + \tfrac{3}{5}c - (\tfrac{3}{5})^{3/2}d + \tfrac{9}{25}e - (\tfrac{3}{5})^{5/2}f) + \tfrac{8}{9}(a) \\ + \tfrac{5}{9}(a + (\tfrac{3}{5})^{1/2}b + \tfrac{3}{5}c + (\tfrac{3}{5})^{3/2}d + \tfrac{9}{25}e + (\tfrac{3}{5})^{5/2}f). \end{aligned} \tag{13}$$

We can sum the fractions and obtain

$$\int_{-1}^{1} p_5(x)dx = \tfrac{8}{9}a + 2 \times \tfrac{5}{9}(a + \tfrac{3}{5}c + \tfrac{9}{25}e) = 2a + \tfrac{2}{3}c + \tfrac{2}{5}e. \tag{14}$$

Hence, the expressions from using quadrature points and weights and from direct integration are identical, so the method is correct for all polynomials up to the fifth order.

m	Integral value	Estimated error	Num. of intervals
4	10.8528	1.78×10^{-15}	1
5	20.5775	2.22×10^{-14}	1
6	40.9668	8.03×10^{-8}	16
7	81.0999	5.87×10^{-7}	15
8	163.441	7.38×10^{-7}	20

Table 1: Integral values, estimated error, and number of intervals for the 3-point adaptive Gauss quadrature scheme applied to the integral $\int_{-1}^{9/4}(x^m - x^2 + 1)dx$ for various values of m.

Integral	Integral value	Estimated error	Num. of intervals
$\int_{-1}^{1} \lvert x\rvert dx$	1	0	2
$\int_{-1}^{2} \lvert x\rvert dx$	2.50000	7.2055×10^{-11}	16
$\int_{0}^{1} x^{4/5} \sin \frac{1}{x} dx$	0.40115	2.2733×10^{-7}	91426

Table 2: Integral values, estimated error, and number of intervals for four sample integrals, using the 3-point adaptive Gauss quadrature scheme.

Part (b) – adaptive integration through 3 point Gauss quadrature

We now implement the adaptive scheme using 3-point Gauss quadrature as discussed in part (a)—see the attached code examples for details. For the integrals of the form

$$\int_{-1}^{9/4}(x^m - x^2 + 1)dx, \tag{15}$$

the computed values, estimated error, and number of intervals are given in Table 1. As expected from part (a), the integrals for $m = 4$ and $m = 5$ are computed exactly with a single integration step. The integrals for $m \geq 6$ are determined to high accuracy with a small number of subdivisions of the interval.

Part (c) – sample integrals

We use the same integration routine to compute the integrals given in this problem. The answers are tabulated in Table 2.

Problem 3 – integration of a family of functions

Figure 2(a) shows a plot of the function $g(x; \frac{1}{3})$. The recursive construction of g results in a function with many peaks in a fractal arrangement that is reminiscent of the Koch curve.[†] Figure 2(b) shows a plot of $g(x, \phi)$ for twenty six different values of ϕ in the range from 0 to $\frac{1}{2}$. For $\phi = 0$, $g(x; \phi) = |x|$ since all of the ϕ^k terms vanish. For $\phi = \frac{1}{2}$, the graph

[†] https://en.wikipedia.org/wiki/Koch_snowflake

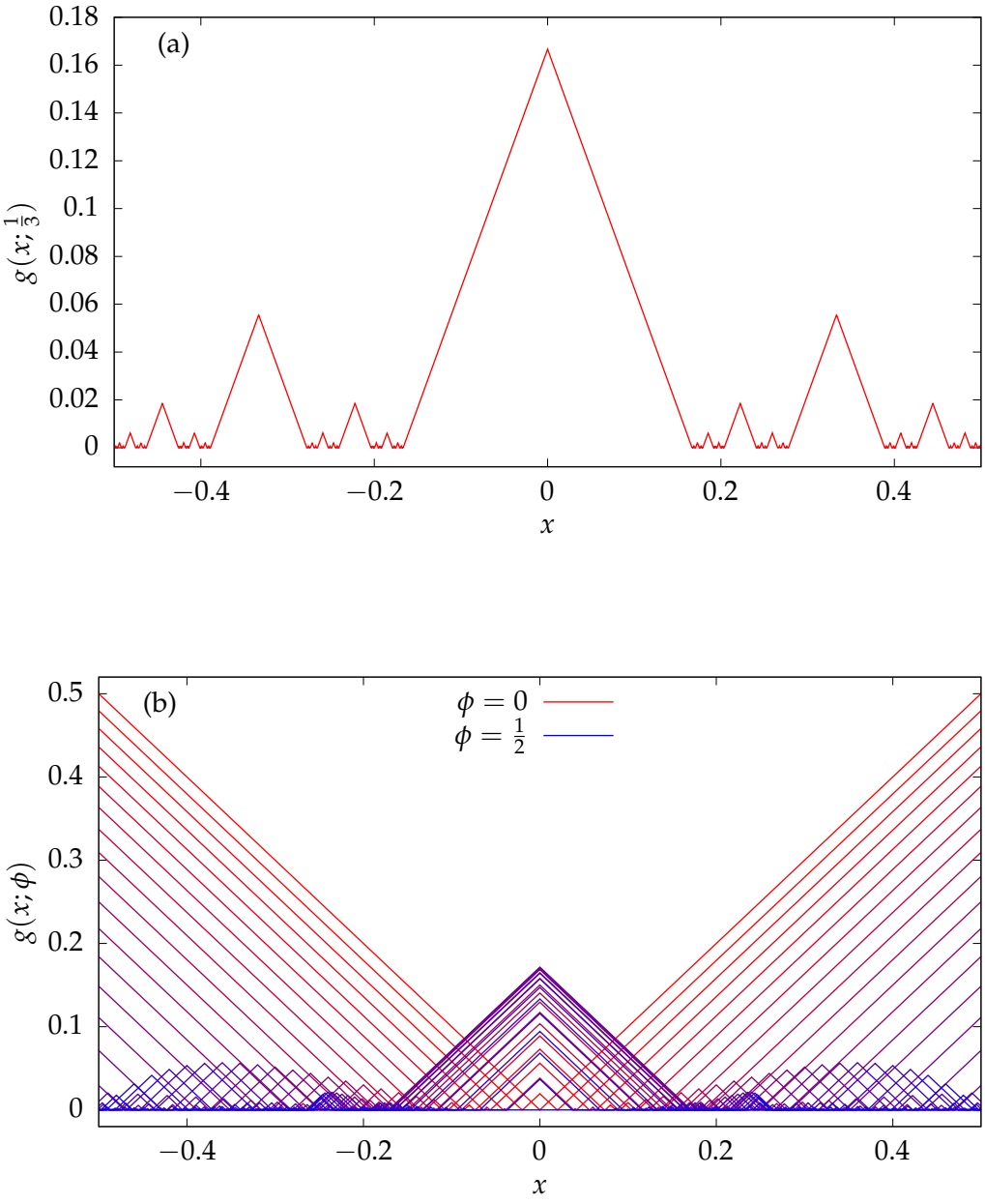

Figure 2: (a) Plot of $g(x;\frac{1}{3})$. (b) Plot of $g(x,\phi)$ for a range of values of ϕ, using a gradation of colors from $\phi = 0$ to $\phi = \frac{1}{2}$.

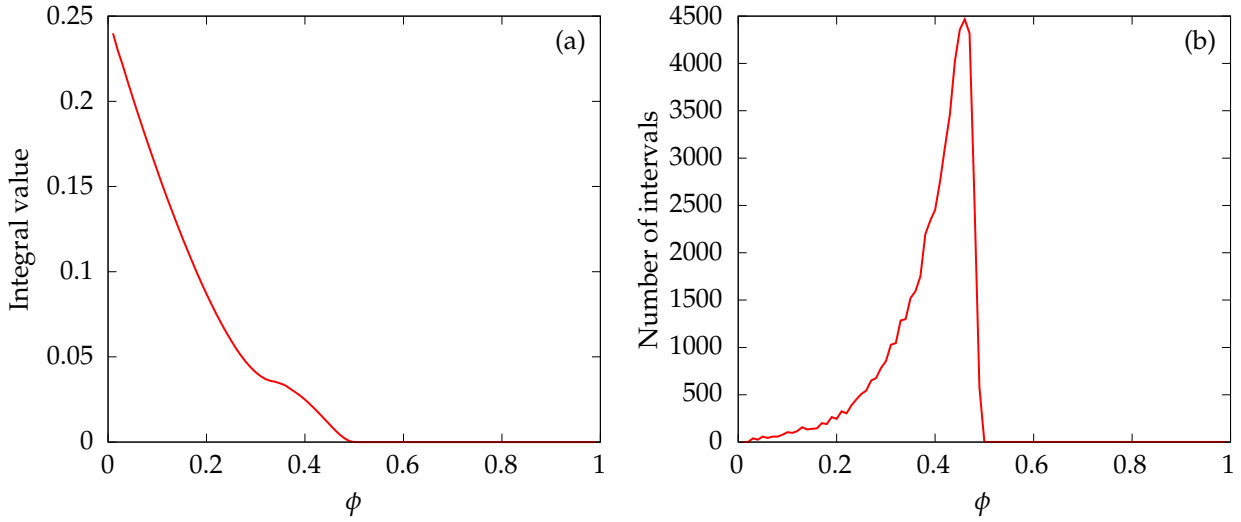

Figure 3: (a) Plot of the integral $\int_{-1/2}^{1/2} g(x;\phi)dx$ as a function of ϕ. (b) Plot of the number of integration intervals required to compute the integral to the desired tolerance of 10^{-6}.

shows that $g(x;\phi) = 0$, which can be verified by induction. Suppose that $x \in [-\frac{1}{2}, \frac{1}{2}]$. Then $0 \leq f_0(x) \leq \frac{1}{2}$. Hence $-\frac{1}{2} \leq f_0(x) - \frac{1}{2} \leq 0$ and thus $f_1(x) = |f_0(x) - \frac{1}{2}| \leq \frac{1}{2}$. Now consider the induction step, and suppose that $0 \leq f_{k-1}(x) \leq 2^{-k-1}$. Then subtracting 2^{-k} from the inequalities yields

$$-\frac{1}{2^k} \leq f_{k-1}(x) - \frac{1}{2^k} \leq \frac{1}{2^k} \tag{16}$$

and hence

$$0 \leq f_k(x) = \left| f_{k-1}(x) - \frac{1}{2^k} \right| \leq \frac{1}{2^k}. \tag{17}$$

Therefore by induction this must hold for every k and thus $g(x) = \lim_{k\to\infty} |f_k(x)| = 0$.

Figure 3(a) shows a plot of the integral value as a function of ϕ. As expected the integral decreases to zero at $\phi = \frac{1}{2}$. Figure 3(b) shows the number of intervals needed to compute the integral to the given tolerance level, which highlights that the most intervals are needed for ϕ in the range $[0.4, 0.5]$. Comparing with Fig. 2 shows that this range has a large number of peaks, which require many interval subdivisions in order to achieve the desired level of accuracy.

Problem 4 – error analysis of a numerical integration rule

Part (a)

We want to use Taylor series to prove the midpoint method

$$y_{k+1} = y_k + hf\left(t_{k+1/2}, \frac{y_k + y_{k+1}}{2}\right) \tag{18}$$

converges as a function of h^2, where $h = t_{k+1} - t_k$. We expand $y(t_{k+1})$ and $y(t_k)$ around $t_{k+1/2}$ and obtain

$$\begin{aligned} y(t_{k+1}) &= y(t_{k+1/2}) + \frac{h}{2}y'(t_{k+1/2}) + \frac{h^2}{8}y''(t_{k+1/2}) + O(h^3)y'''(t_{k+1/2}), \\ y(t_k) &= y(t_{k+1/2}) - \frac{h}{2}y'(t_{k+1/2}) + \frac{h^2}{8}y''(t_{k+1/2}) + O(h^3)y'''(t_{k+1/2}) \end{aligned} \tag{19}$$

We arrive at

$$\frac{y(t_{k+1}) - y(t_k)}{h} = y'(t_{k+1/2}) + O(h^2)y'''(t_{k+1/2}). \tag{20}$$

We can also expand $f(t_{k+1/2}, \frac{y(t_k)+y(t_{k+1})}{2})$ around $t_{k+1/2}$ and obtain

$$\begin{aligned} f\left(t_{k+1/2}, \tfrac{y(t_k)+y(t_{k+1})}{2}\right) &= f\left(t_{k+1/2}, y(t_{k+1/2}) + \tfrac{y(t_k)+y(t_{k+1})}{2} - y(t_{k+1/2})\right) \\ &= y'(t_{k+1/2}) + \left(\frac{y(t_k)+y(t_{k+1})}{2} - y(t_{k+1/2})\right)\left.\frac{\partial f}{\partial y}\right|_{y_{(t_{k+1/2})}} \\ &\quad + O\left(\frac{y(t_k)+y(t_{k+1})}{2} - y(t_{k+1/2})\right)^2 \left.\frac{\partial^2 f}{\partial y^2}\right|_{y_{(t_{k+1/2})}}. \end{aligned} \tag{21}$$

We can plug in the Taylor expansion of $y(t_k)$ and $y(t_{k+1})$ around $y(t_{k+1/2})$ to obtain

$$\frac{y(t_k)+y(t_{k+1})}{2} - y(t_{k+1/2}) = \frac{h^2}{8}y''(t_{k+1/2}) + O(h^3)y'''(t_{k+1/2}). \tag{22}$$

As a result, we arrive at the expression

$$f\left(t_{k+1/2}, \tfrac{y(t_k)+y(t_{k+1})}{2}\right) = y'(t_{k+1/2}) + \left.\frac{\partial f}{\partial y}\right|_{y_{(t_{k+1/2})}} (\frac{h^2}{4}y''(t_{k+1/2}) + O(h^3)y'''(t_{k+1/2})). \tag{23}$$

Using Eqs. 20 and 23, we aim to compute the truncation error T_k, which gives the convergence rate of the method as we invoke the theorem discussed in lecture. The truncation error is given by

$$T_k = \frac{y(t_{k+1}) - y(t_k)}{h} - f\left(t_{k+1/2}, \frac{y(t_k)+y(t_{k+1})}{2}\right) \tag{24}$$

and hence

$$T_k = y'(t_{k+1/2}) + O(h^3)y'''(t_{k+1/2}) - y'(t_{k+1/2}) \\ - \left.\frac{\partial f}{\partial y}\right|_{y_{(t_{k+1/2})}} \left(\frac{h^2}{4}y''(t_{k+1/2}) + O(h^3)y'''(t_{k+1/2})\right). \tag{25}$$

Therefore T_k is $O(h^2)$ and the method is second-order accurate.

Stability region of midpoint method

We want to find the stability region of the midpoint method for the ode $y' = \lambda y$. We plug the differential equation into the midpoint method and obtain

$$y_{k+1} = y_k + h\lambda\left(\frac{y_k + y_{k+1}}{2}\right). \tag{26}$$

Rearranging the equation leads to

$$y_{k+1}\left(1 - \frac{h\lambda}{2}\right) = y_k\left(1 + \frac{h\lambda}{2}\right), \tag{27}$$

which can be rewritten as

$$y_{k+1} = \left(\frac{1 + \bar{h}/2}{1 - \bar{h}/2}\right) y_k, \tag{28}$$

where $\bar{h} = h\lambda \in \mathbb{C}$. This equation is stable if and only if

$$\left|\frac{1 + \bar{h}/2}{1 - \bar{h}/2}\right| \leq 1. \tag{29}$$

If $\bar{h}$ is written in terms of real and imaginary parts as $\bar{h} = a + ib$ then

$$\left(1 + \tfrac{a}{2}\right)^2 + b^2 \leq \left(1 - \tfrac{a}{2}\right)^2 + b^2 \tag{30}$$

and hence

$$a \leq -a, \tag{31}$$

which implies $a \leq 0$ and $b \in \mathbb{R}$. Hence, the asymptotically stable case is when $\bar{h}$ is the imaginary axis. Anywhere left of the imaginary axis gives strictly converging case. Hence, to have convergence, the discretization of the differential equation must satisfy the $\operatorname{Re}\bar{h} \leq 0$. Figure 4 shows the stability region.

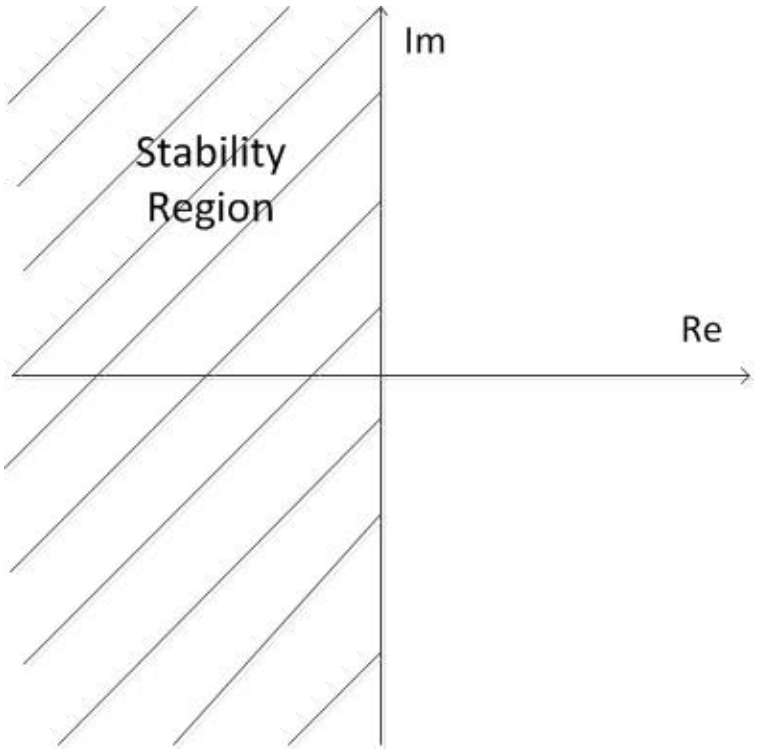

Figure 4: Stability region of midpoint method.

Problem 5 – a multi-step method

Part (a)

The numerical method is based on approximating $f(t, y)$ using the four-point Lagrange interpolation

$$f_{\text{approx}}(t, y) = f_{k-2}L_{k-2}(t) + f_{k-1}L_{k-1}(t) + f_k L_k(t) + f_{k+1}L_{k+1}(t). \tag{32}$$

where the L_l are (cubic) Lagrange polynomials that are one at corresponding t_l and zero at the other control points. If a new time variable s is introduced so that $t = t_k + hs$, then the numerical scheme becomes

$$y_{k+1} = y_{k-1} + h\int_{-1}^{1} f_{\text{approx}}(t_k + hs, y)ds. \tag{33}$$

To proceed, consider the integrals of the Lagrange polynomials:

$$\int_{-1}^{1} L_{k-2}(t_k + hs)ds = \frac{1}{-6}\int_{-1}^{1}(s-1)s(s+1)ds = 0, \tag{34}$$

$$\int_{-1}^{1} L_{k-1}(t_k + hs)ds = \frac{1}{2}\int_{-1}^{1}(s-1)s(s+2)ds = \frac{1}{3}, \tag{35}$$

$$\int_{-1}^{1} L_{k}(t_k + hs)ds = \frac{1}{-2}\int_{-1}^{1}(s-1)(s+1)(s+2)ds = \frac{4}{3}, \tag{36}$$

$$\int_{-1}^{1} L_{k+1}(t_k + hs)ds = \frac{1}{6}\int_{-1}^{1}s(s+1)(s+2)ds = \frac{1}{3}. \tag{37}$$

Note that the integral of L_{k-2} vanishes because of symmetry. This is an advantage, since it ensures that the numerical scheme will achieve a higher order of accuracy, with one fewer function evaluation. Hence Eq. 33 becomes

$$y_{k+1} = y_{k-1} + \frac{h}{3}\left(f_{k-1} + 4f_k + f_{k+1}\right). \tag{38}$$

Part (b)

To solve the differential equation

$$y''(t) + 2y'(t) + 17y(t) = 0. \tag{39}$$

with initial conditions $y(0) = 1, y'(0) = 0$, consider a possible solution of $y = e^{mt}$. To be a solution, the parameter m must satisfy

$$m^2 + 2m + 17 = 0, \tag{40}$$

which can also be written as

$$(m+1)^2 = -16. \tag{41}$$

This has two solutions, $m = -1 \pm 4i$. Hence, the general solution has the form

$$y(t) = e^{-t}(A\cos 4t + B\sin 4t) \tag{42}$$

where A and B are constants. The first derivative is

$$y'(t) = e^{-t}((4B - A)\cos 4t - (4A + B)\sin 4t) \tag{43}$$

and hence

$$y(0) = A, \qquad y'(0) = 4B - A. \tag{44}$$

Hence $A = 1$ and $B = \frac{1}{4}$ to satisfy the initial conditions.

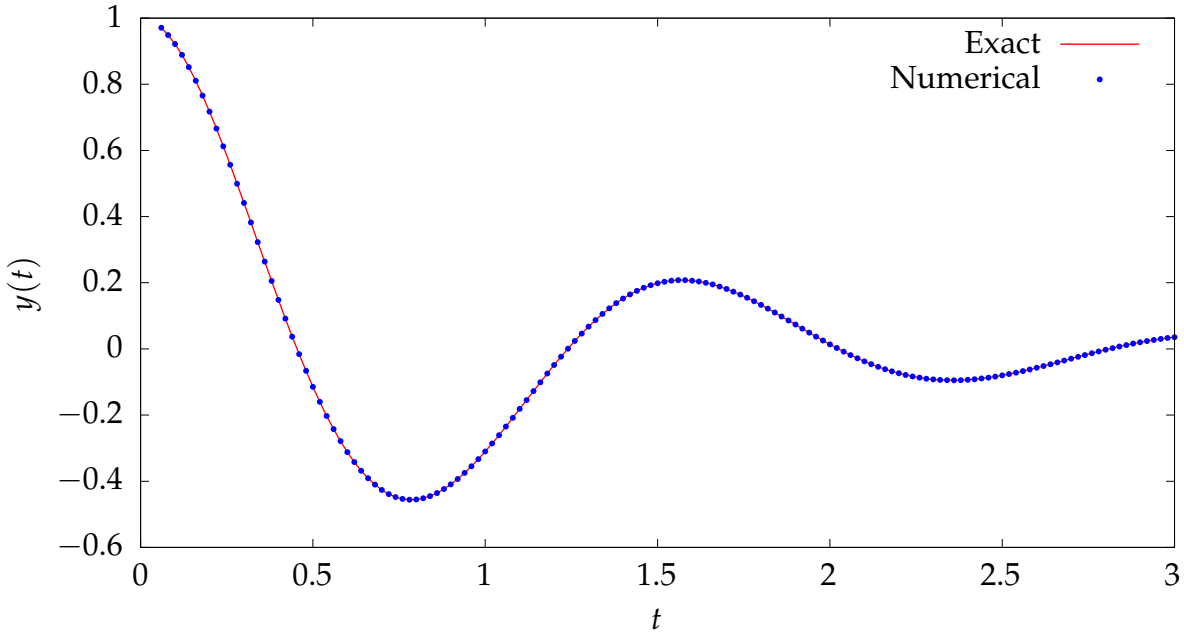

Figure 5: Comparison between the exact solution and the numerical solution using the Nyström method, for the ODE considered in problem 5.

Part (c)

By defining $y' = v$, the differential equation in Eq. 39 becomes a first-order system,

$$y' = v, \qquad v' = -2v - 17y \tag{45}$$

Equivalently, this is

$$\begin{pmatrix} y' \\ v' \end{pmatrix} = \begin{pmatrix} 0 & 1 \\ -17 & -2 \end{pmatrix} \begin{pmatrix} y \\ v \end{pmatrix}, \tag{46}$$

or $\mathbf{y}' = A\mathbf{y}$ where $\mathbf{y} = (y, v)$ and

$$A = \begin{pmatrix} 0 & 1 \\ -17 & -2 \end{pmatrix}. \tag{47}$$

Hence, for this system, the Nyström method of Eq. 38 is

$$\mathbf{y}_{k+1} = \mathbf{y}_{k-1} + \frac{h}{3}\left(A\mathbf{y}_{k-1} + 4A\mathbf{y}_k + A\mathbf{y}_{k+1}\right). \tag{48}$$

Collecting the terms involving $\mathbf{y}_{k+1}$ yields

$$\mathbf{y}_{k+1} - \frac{hA}{3}\mathbf{y}_{k+1} = \mathbf{y}_{k-1} + \frac{h}{3}\left(A\mathbf{y}_{k-1} + 4A\mathbf{y}_k\right), \tag{49}$$

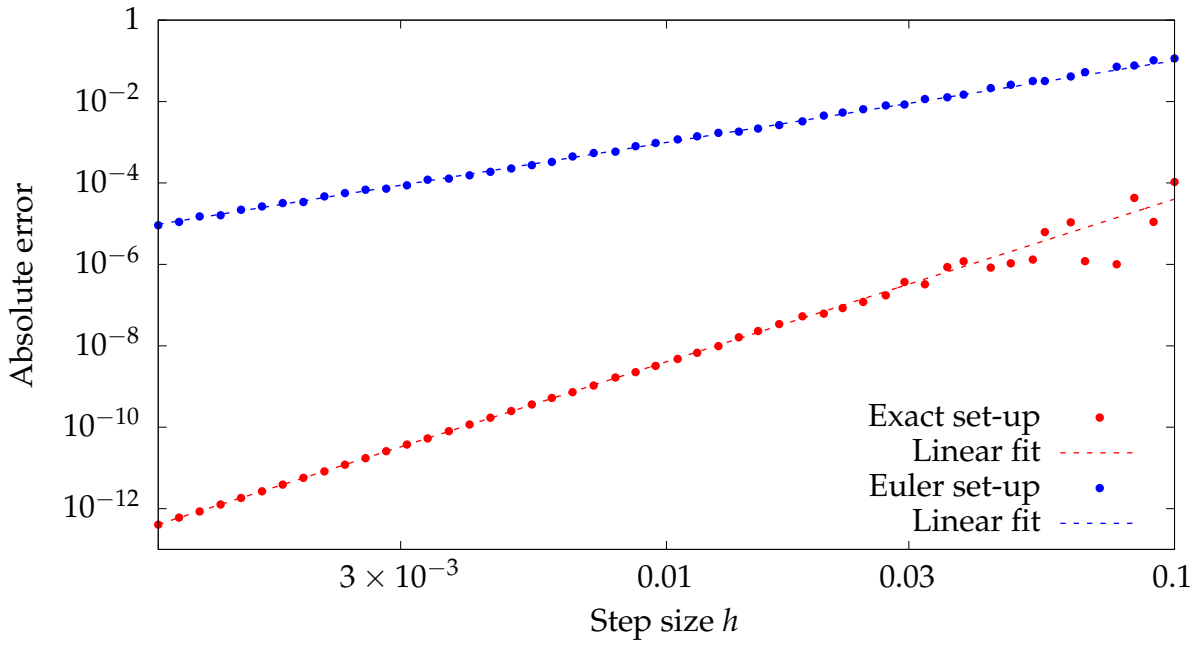

Figure 6: Graph showing the absolute error between the exact and numerical solutions at $t = 3$ a function of the step size h, for the ODE considered in problem 5. The graph shows the absolute errors for the case when the first two steps are set using the exact solution, and for the case when they are set using Euler steps. In each case a line of best fit, fitted over the range $10^{-3} \leq h \leq 10^{-2}$, is shown.

and hence

$$\mathbf{y}_{k+1} = \left(1 - \frac{hA}{3}\right)^{-1} \left(\left(1 + \frac{Ah}{3}\right)\mathbf{y}_{k-1} + \frac{4Ah}{3}\mathbf{y}_k\right). \tag{50}$$

This is now an explicit formula for $\mathbf{y}_{k+1}$ in terms of the previous values of $\mathbf{y}$. The program `q5.py` implements this numerical scheme. Figure shows the exact and numerical solutions and demonstrates that they are near-identical.

Figure 6 shows a log–log plot of the absolute error between the exact and numerical $\mathbf{y}$ for a variety of step sizes between $h = 10^{-1}$ and $h = 10^{-3}$. The plot also contains a line of best fit, which has a slope of 3.995, confirming that the method is fourth-order accurate. It is worth noting that the method is a remarkably efficient way to achieve fourth-order accuracy, since it only requires considering the previous two values at each step.

Part (d)

Figure 6 also shows the absolute error between the exact and numerical solutions when $\mathbf{y}_1$ and $\mathbf{y}_2$ are set using an Euler step. Second-order accuracy is observed, with the best-fit line having slope of 2.009. This should be expected since the truncation error of the Euler method is $O(h)$. Since two steps of size h are taken to determine $\mathbf{y}_1$ and $\mathbf{y}_2$, the local error

incurred is $O(h^2)$. The error on these first two steps will dominate the global error at $t = 3$.

Problem 6 – asteroid collision

Part (a)

The Jacobi integral is

$$J(x, y, u, v) = (x + \mu)^2 + y^2 + \frac{2(1-\mu)}{\sqrt{x^2+y^2}} + \frac{2\mu}{\sqrt{(x-1)^2+y^2}} - u^2 - v^2. \tag{51}$$

The asteroid's equations of motion are given by the partial derivatives of J,

$$\begin{aligned} x' &= u, \\ y' &= v, \\ u' &= v + (x - \mu) - \frac{(1-\mu)x}{(x^2+y^2)^{3/2}} - \frac{\mu(x-1)}{((x-1)^2+y^2)^{3/2}}, \\ v' &= -u + y - \frac{(1-\mu)y}{(x^2+y^2)^{3/2}} - \frac{\mu y}{((x-1)^2+y^2)^{3/2}}. \end{aligned} \tag{52}$$

Part (b)

Consider a line segment between two points $\mathbf{x}_1$ and $\mathbf{x}_2$, and define $\Delta\mathbf{x} = \mathbf{x}_2 - \mathbf{x}_1$. Consider the infinite line

$$\mathbf{x} = \mathbf{x}_1 + \lambda\Delta\mathbf{x} \tag{53}$$

where $\lambda \in \mathbb{R}$. The value of λ that minimizes the distance of $\mathbf{x}$ from the origin is given by projecting out part of $\mathbf{x}_1$ in the direction of Δx. This is given in terms of scalar products as

$$\lambda = -\frac{\mathbf{x}_1 \cdot \Delta\mathbf{x}}{\Delta\mathbf{x} \cdot \Delta\mathbf{x}}. \tag{54}$$

If $\lambda \in [0, 1]$, then this point will on the line segment between $\mathbf{x}_1$ and $\mathbf{x}_2$. If $\lambda < 0$, then the closest point on the segment to the origin will be $\mathbf{x}_1$. If $\lambda > 1$, then the closest point on the segment to the origin will be $\mathbf{x}_2$.

Define this closest point is $\mathbf{x}_{\text{min}}$. If $|\mathbf{x}_{\text{min}}| < R$ then the line segment intersects the circle of radius R at the origin. Otherwise, it does not intersect. This calculation is incorporated in the `detect` function in the program `threebody.py` that is used in the subsequent sections.

Parts (c) and (d)

If the trajectory is assumed to be linear from $t = 0$ to $t = 0.02$, then the velocity at $t = 0$ is

$$\mathbf{v}(0) = \frac{\mathbf{x}(0.02) - \mathbf{x}(0)}{0.02}. \tag{55}$$

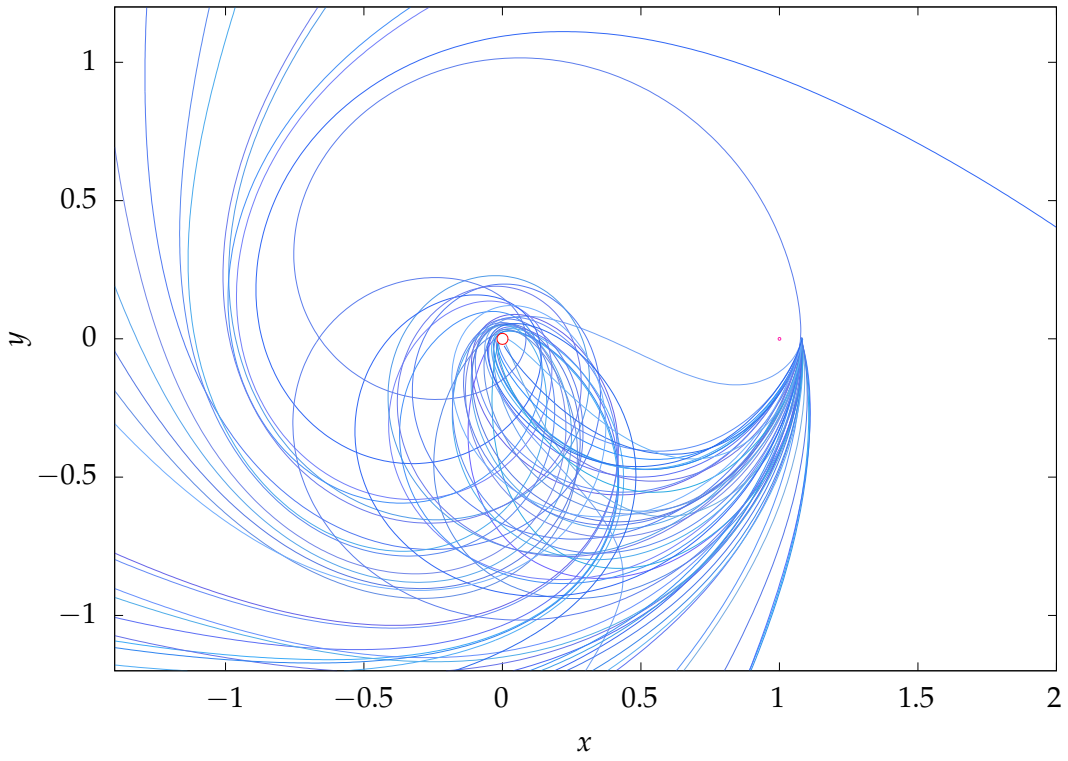

Figure 7: Fifty possible asteroid trajectories. The Earth is the circle at the origin, and the Moon is the circle at $(1, 0)$.

The program `threebody.py` performs integrations of the asteroid trajectory using samples drawn from the given initial conditions. Figure 7 shows fifty example trajectories. Of these fifty trajectories, the majority quickly escape the Earth–Moon system, suggesting that this is the most likely scenario.

Figure 8(a) shows 36 trajectories that collide with the Earth. All but one of the trajectories collides with the Earth after a single arc. However, a single trajectory collides by first orbiting around the Moon, demonstrating the possibility of complex interactions in the three-body system. Figure 8(b) shows 36 trajectories that collide with the Moon. The majority undergo several close passes around the Earth, before colliding with the Moon.

Table 3 shows the estimated probabilities of the different scenarios, based on 5×10^8 trials. A trajectory is classified as escaping the Earth–Moon system if $|\mathbf{x}| > 20$. This does not rigorously guarantee that a trajectory will escape, but in practice it is a very good indication. Over the interval $t \in [0, 10]$, one finds that 67.69% of trajectories escape, 25.60% of trajectories collide with the Earth, and 0.1878% of trajectories collide with the Moon. The remaining 6.521% of trajectories persist until $t = 10$, and are analyzed in more detail in part (f).

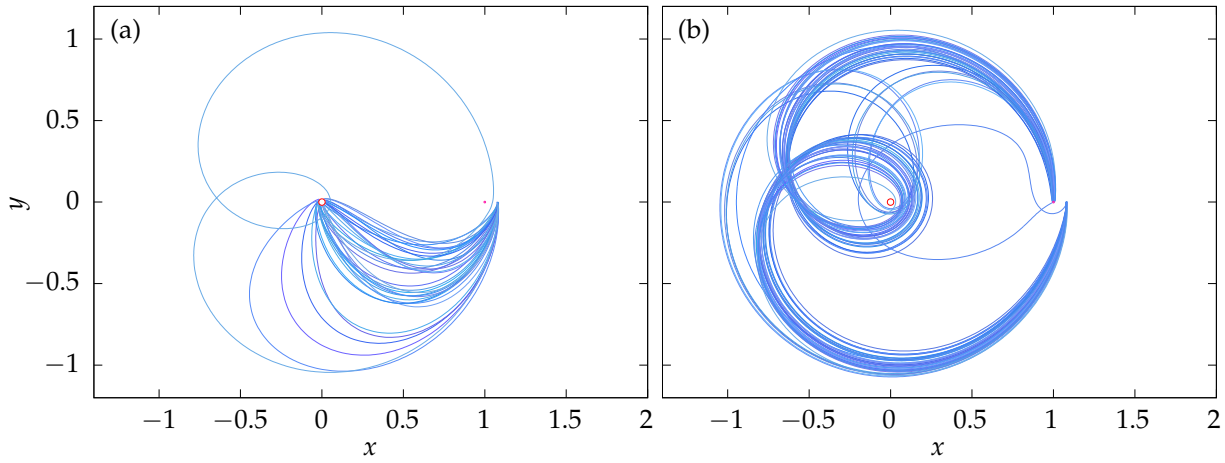

Figure 8: 36 asteroid trajectories that (a) collide with Earth and (b) collide with the Moon. The Earth is the circle at the origin, and the Moon is the circle at $(1, 0)$.

Type	Cases (linear)	Percent	SE	Cases (exact)	Percent	SE
Escape, $t \in [0, 10]$	338,440,422	67.69	0.0021	346,954,316	69.39	0.0021
Earth, $t \in [0, 10]$	128,014,461	25.60	0.0020	118,983,556	23.80	0.0019
Moon, $t \in [0, 10]$	939,012	0.1878	0.00019	942,510	0.1885	0.00019
Escape, $t \in (10, 200]$	32,457,022	6.491	0.0011	32,968,484	6.594	0.0011
Earth, $t \in (10, 200]$	42,920	0.008584	4.1×10^{-5}	46,508	0.009302	4.3×10^{-5}
Moon, $t \in (10, 200]$	52,035	0.01041	4.6×10^{-5}	52,782	0.01056	4.6×10^{-5}
Persistent, $t > 200$	54,128	0.01083	4.7×10^{-5}	51,844	0.01037	4.6×10^{-5}
Total	500,000,000	100	0	500,000,000	100	0

Table 3: Total occurrences of each type of trajectory, based on two sets of 5×10^8 trials. Columns 2–4 contain results for when the asteroid velocity is assumed to be linear between the two observations, and columns 5–7 contain results for when the asteroid velocity is precisely fit so that the trajectory goes through the two observations. For each set of results, the probability of each type of trajectory is reported, along with a measure of standard error (SE) of the measurement. The SE is calculated by assuming the counts follow a binomial distribution.

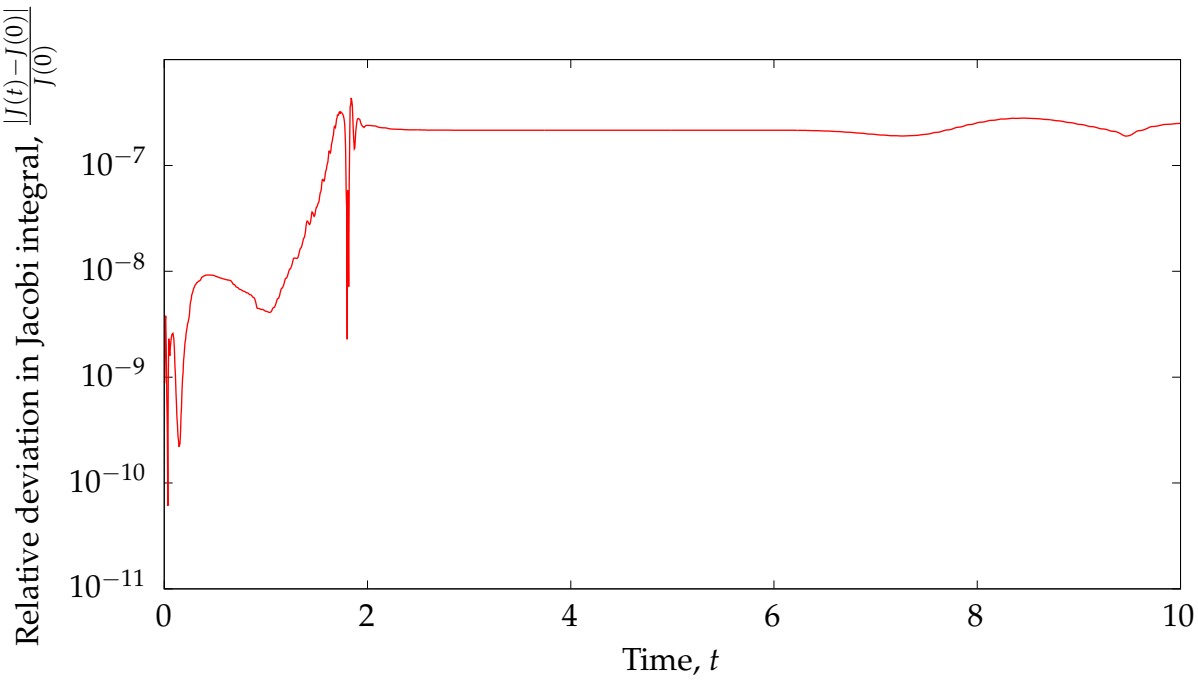

Figure 9: Relative deviation the Jacobi integral for the trajectory where $\mathbf{x}(0) = (1.08, 0)$ and $\mathbf{v}(0) = (0, -0.49)$.

Part (e)

Figure 9 shows a plot of the relative deviation in the Jacobi integral over the time interval from 0 to 10 for the given initial conditions. The relative deviation remains smaller than 10^{-6} throughout the calculation.

Part (f)

For any trajectory that persists until $t = 10$, the `threebody.py` program performs a second integration up to $t = 200$. Over this extended time window, 6.491% escape, 0.008584% collide with the Earth, and 0.01041% collide with the Moon. Interestingly, over this extended time window the probability of colliding with the Moon is higher than colliding with the Earth, which is the opposite of the behavior for $t \in [0, 10]$.

The remaining 0.01083% of trajectories neither escape, nor collide with either body, and are classified as "persistent" in Table 3. To examine the structure of these trajectories in more detail, several different statistics are also stored about them, using the time interval $t \in [10, 190]$. Figure 10 shows a scatter plot of the persistent trajectories in terms of their Jacobi integral, J, and their mean squared distance from the Earth, R_E. Three distinct clusters of trajectory occur, and substantial fine structure is seen the clusters.

One cluster is observed for $J < 2.6$, corresponding to trajectories with a relatively high

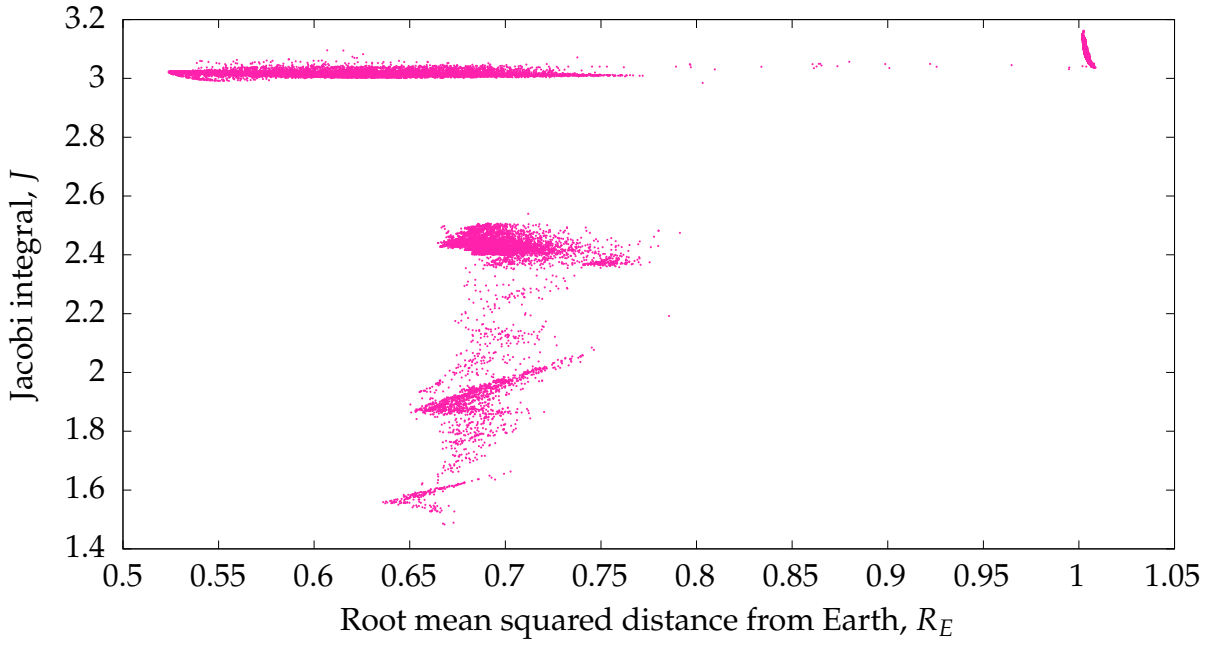

Figure 10: Scatter plot showing all of the asteroid trajectories that persist until $t = 200$, arranged according to their Jacobi integral and root mean squared distance from Earth. 54,128 trajectories are shown, out of the total of 5×10^8 that were simulated.

speed. Figure 11 shows six examples of persistent trajectories in this cluster, indicating that they are Earth orbits, configured in such a way that the Moon does not perturb them. Figs. 11(a) and 11(b) are within a range $[R_{\text{lo}}, R_{\text{hi}}]$ of Earth, where R_{hi} is small enough that the Moon has limited influence. The remaining four examples have a slightly different structure, where the Earth–Moon rotation time is approximately a multiple of the period of the asteroid orbit, meaning that the trajectory appears concentrated in specific broad tracks in the co-rotating frame. Figs. 11(c) and 11(d) show examples of one-lobe and two-lobe tracks, respectively, which are arranged in such a way that the asteroid largely avoids getting close to the Moon, which would likely perturb it. Figs. 11(e) and 11(f) are more random, but weak three-lobe and four-lobe structures, respectively, are visible.

A very tight second cluster is visible in Fig. 10 for $J > 2.6$ and $R_E > 1$. This cluster corresponds to lunar orbits, and two examples are shown in Fig. 12. In the co-rotating frame the orbits appear to precess. In some cases like Fig. 12(a) the orbit traces out a broad swath of space in the co-rotating frame, but in others like Fig. 12(b) the orbit appears locked into a small number of distinct tracks. It is not clear whether Fig. 12(b) is purely coincidental or if resonances due to the Earth cause this behavior.

The final cluster visible in Fig. 10 has $J > 2.6$ and $R_E < 1$ and corresponds to trajectories with complex Earth–Moon interactions. Figure 13 shows six examples. Fig. 13(a) shows an example with a high R_E, where the asteroid first orbits the Moon but is eventually

perturbed and enters an Earth orbit. Figs. 13(b–e) show other examples, where the asteroid orbits the Earth, but occasionally encounters the Moon, often perturbing it into a different orbital configuration. Figure 13(f) shows a very special extreme example at $(R_E, J) = (0.8031, 2.986)$, which is visible as an isolated point outside of the cluster in Fig. 10. This trajectory undergoes a very large elliptical orbit that forms a six-fold pattern in the co-rotating frame, which is arranged in such a way that it avoids getting too close to the Moon.

It is likely that most of the trajectories shown in Fig. 10 are not truly stable, but take advantage of very special coincidences—it is worth recalling that only 0.01% of the total trajectories fall into this category. The trajectories in Fig. 13 are particularly likely to be perturbed, since at some point an interaction with the Moon may cause the asteroid to escape, or set it on a collision course.

Part (g)

The previous results all calculate the asteroid's initial velocity $\mathbf{v}(0)$ assuming that it is linear between the two observations. However, in reality, it will follow a curved path. The `threebody.py` program has an option to take this into account, so that $\mathbf{v}(0)$ is chosen to ensure that the real trajectory precisely passes through $\mathbf{x}(0.02)$. This is done by introducing a functional

$$\mathbf{F}(\mathbf{v}) = \mathbf{x}(0.02) - \mathbf{x}_{\text{test}}(\mathbf{v}, 0.02), \tag{56}$$

where $\mathbf{x}_{\text{test}}(\mathbf{v}, 0.02)$ is the numerically computed position at $t = 0.02$ using $\mathbf{v}$ is the initial velocity. Given two observations $\mathbf{x}(0)$ and $\mathbf{x}(0.02)$, the Python routine `root` is used to find the appropriate $\mathbf{v}$ such that $\mathbf{F}(\mathbf{v}) = \mathbf{0}$. It uses Eq. 55 is the initial guess for $\mathbf{v}$, which is usually close to the exact solution.

A second set of five hundred million trials was performed with the improved set-up routine. In these tests, it was found that the `root` algorithm works very reliably and quickly. However, in 540 out of 5×10^8 cases, the algorithm fails to find a solution. In those cases, the initial velocity is chosen using Eq. 55 as a fall-back option.

Table 3 also shows the probabilities of each scenario for this second set. The probabilities shift by small amounts, with the probability of escape increasing from 67.69% to 69.39%. Given the large number of trials the standard errors of these statistics are much smaller than the sizes of the shifts. Hence, the shifts are statistically significant.

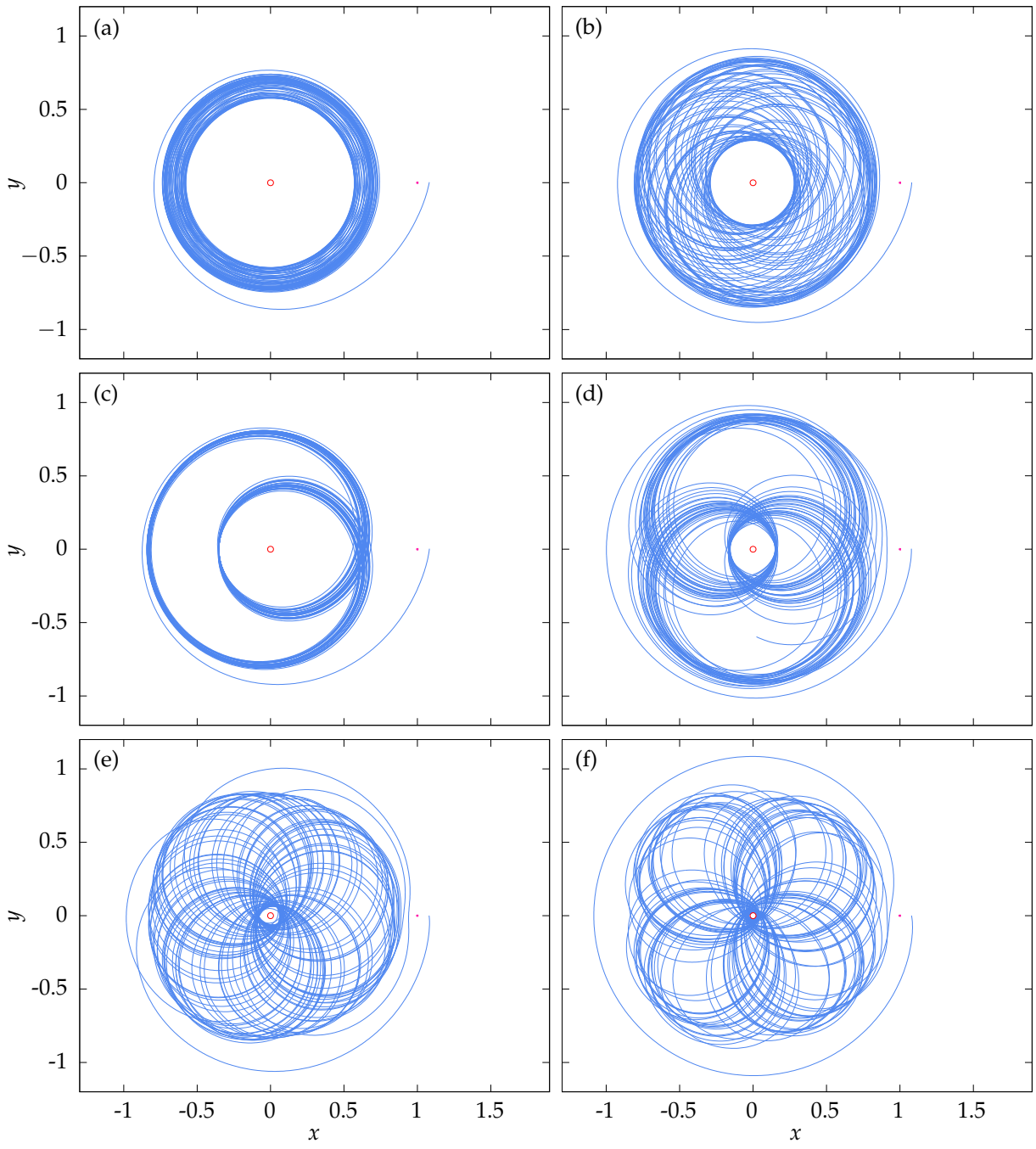

Figure 11: Examples of the first class of persistent trajectories that last until $t = 200$. This class broadly contains trajectories that orbit the Earth with minimal influence from the Moon.

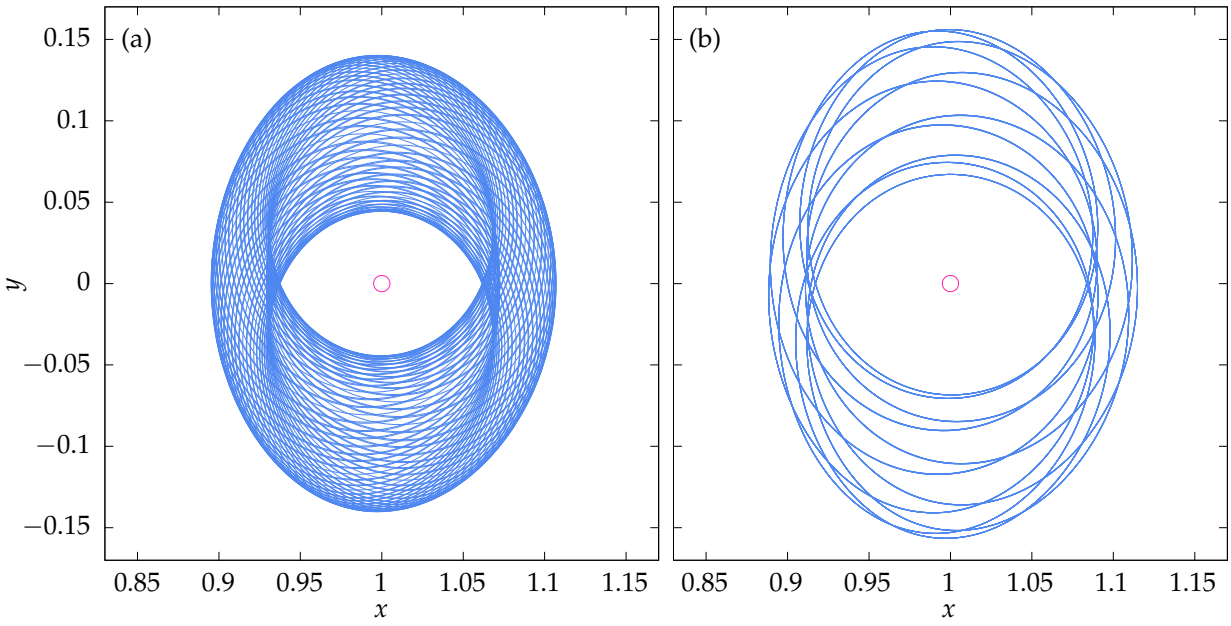

Figure 12: Examples of the second class of persistent trajectories that last until $t = 200$. This class broadly contains trajectories that orbit the Moon.

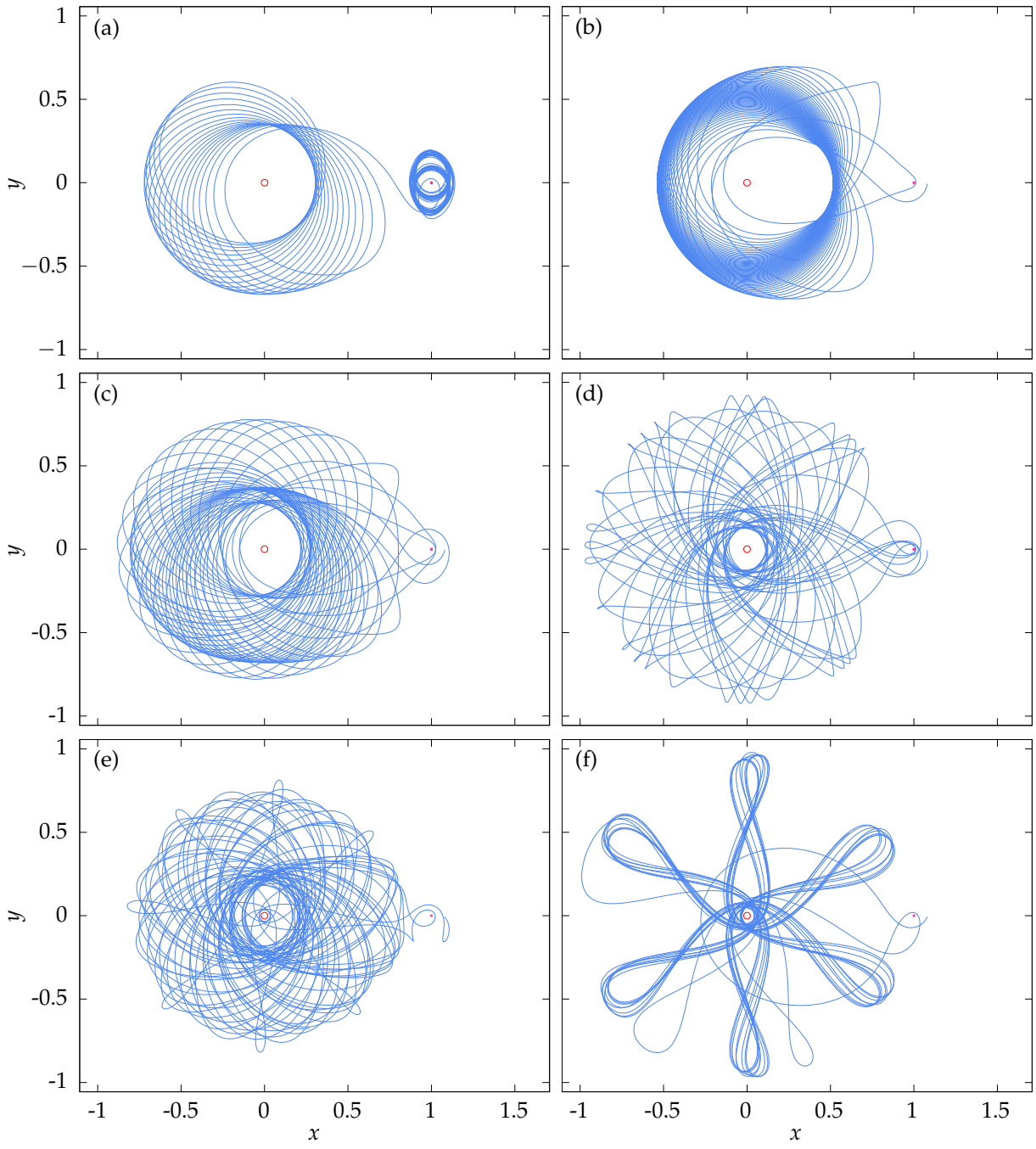

Figure 13: Examples of the third class of persistent trajectories that last until $t = 200$. This class broadly contains trajectories that undergo complex Earth–Moon interactions.